Materials Chemistry and Physics 213 (2018) 285–294

Contents lists available at ScienceDirect

Materials Chemistry and Physics

journal homepage: www.elsevier.com/locate/matchemphys

Characterization, antibacterial and cytotoxicity studies of graphene-Fe_3O_4 nanocomposites and Fe_3O_4 nanoparticles synthesized by a facile solvothermal method

A. Nayamadi Mahmoodabadi [a], A. Kompany [a, b, *], M. Mashreghi [b, c]

[a] Materials and Electroceramics Lab, Department of Physics, Ferdowsi University of Mashhad, Mashhad, Iran
[b] Nano Research Center, Ferdowsi University of Mashhad, Mashhad, 9177948974, Iran
[c] Department of Biology, Ferdowsi University of Mashhad, Mashhad, 9177948974, Iran

HIGHLIGHTS

- Synthesis of graphene-Fe_3O_4 nanocomposites and Fe_3O_4 NPs, by solvothermal method.
- XRD analysis confirmed formation of the desired structure and reduction of graphene.
- Antibacterial investigation by: MIC, colony counting and growth curves methods.
- High antibacterial activity and low toxicity of G-Fe_3O_4 with 1–5 wt ratio.

GRAPHICAL ABSTRACT

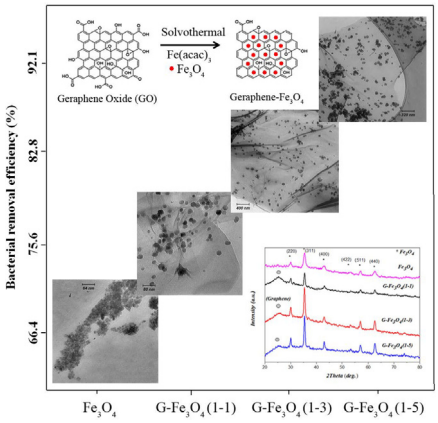

ARTICLE INFO

Article history:
Received 2 July 2017
Received in revised form
28 January 2018
Accepted 7 April 2018
Available online 9 April 2018

Keywords:
Solvothermal
Fe_3O_4 nanoparticles
G-Fe_3O_4 nanocomposites
Antibacterial property
Cytotoxicity

ABSTRACT

Graphene-Fe_3O_4 (G-Fe_3O_4) nanocomposites with different GO/Fe_3O_4 weight ratios of 1-1, 1–3 and 1–5 were synthesized using solvothermal method. Also, Fe_3O_4 nanoparticles (NPs) were separately synthesized by the same method. The prepared samples were characterized by X-ray diffraction (XRD), transmission electron microscopy (TEM) and Fourier transform infrared (FTIR) spectroscopy. Zeta potential analysis and scanning electron microscopy (SEM) were employed to measure the surface charge and the destruction processes of the bacteria. The XRD analysis showed that the graphene oxide had been reduced and also confirmed the formation of G-Fe_3O_4 nanocomposites. The antibacterial properties of the prepared samples were investigated against *Escherichia coli* (ATCC 25922) and *Staphylococcus aureus* (ATCC 25923) strains, using three different methods. Our results revealed that the G-Fe_3O_4 with 1–5 wt ratio has higher antibacterial activity and lower toxicity, compared to the other two nanocomposite samples, GO and also Fe_3O_4 NPs.

1. Introduction

In recent years, the safety of drinking water resources has attracted much attention with regards to the human health and

* Corresponding author. Materials and Electroceramics Lab, Department of Physics, Ferdowsi University of Mashhad, Mashhad, Iran.
E-mail address: kompany@um.ac.ir (A. Kompany).

https://doi.org/10.1016/j.matchemphys.2018.04.033
0254-0584/

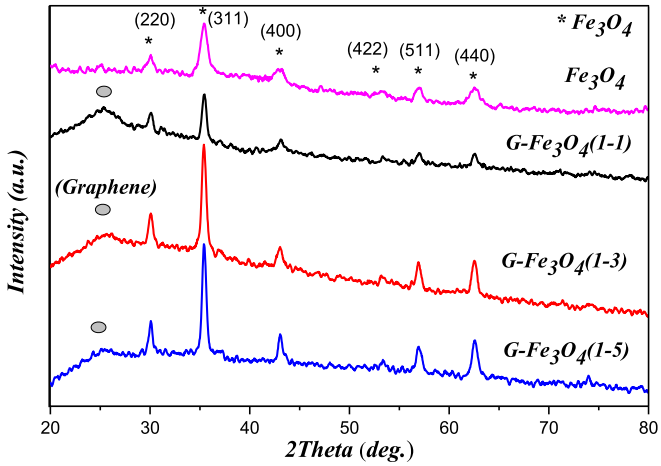

Fig. 1. XRD patterns of the synthesized G-Fe_3O_4 nanocomposites and Fe_3O_4 nanoparticle samples.

environment. Since bacterial infection is an important factor in water pollution, there is a critical need to develop more convenient techniques and use new effective materials to remove and eliminate the bacteria [1,2]. Organic materials, which are used extensively for this purpose, have some disadvantages including toxicity

Table 1
Crystallite size and strain of the synthesized samples.

Compound	Crystallite size		
	Scherrer	SSP	
	D (nm)	D (nm)	$\varepsilon \times 10^{-3}$
G-Fe_3O_4 (1–5)	19.6	22.9	1.60
G-Fe_3O_4 (1–3)	19.3	16.9	0.49
G-Fe_3O_4 (1-1)	19.0	17.0	−0.56
Fe_3O_4	7.7	9.5	−0.28

which is harmful to the human body and the environment [3]. There are more interests in antiseptic inorganic materials such as metal oxide nanoparticles, because of their specific size and shape [4–7]. Furthermore, some ferromagnetic and super paramagnetic nanoparticles, such as Fe_3O_4 NPs, with low toxicity and excellent biocompatibility [8,9] have been used for drug delivery, pollution catalysis and magnetic resonance imaging [10–12]. However, the high magnetic property of Fe_3O_4 NPs causes the agglomeration of the particles, which makes it difficult to control the monodispersed size of the nanocrystals. One way to solve this problem is to distribute the NPs on a suitable support such as graphene-based materials [13]. Graphene is a two-dimensional single sheet of carbon atoms arranged in a hexagonal network, which can be obtained through micromechanical or chemical exfoliation of graphite. The

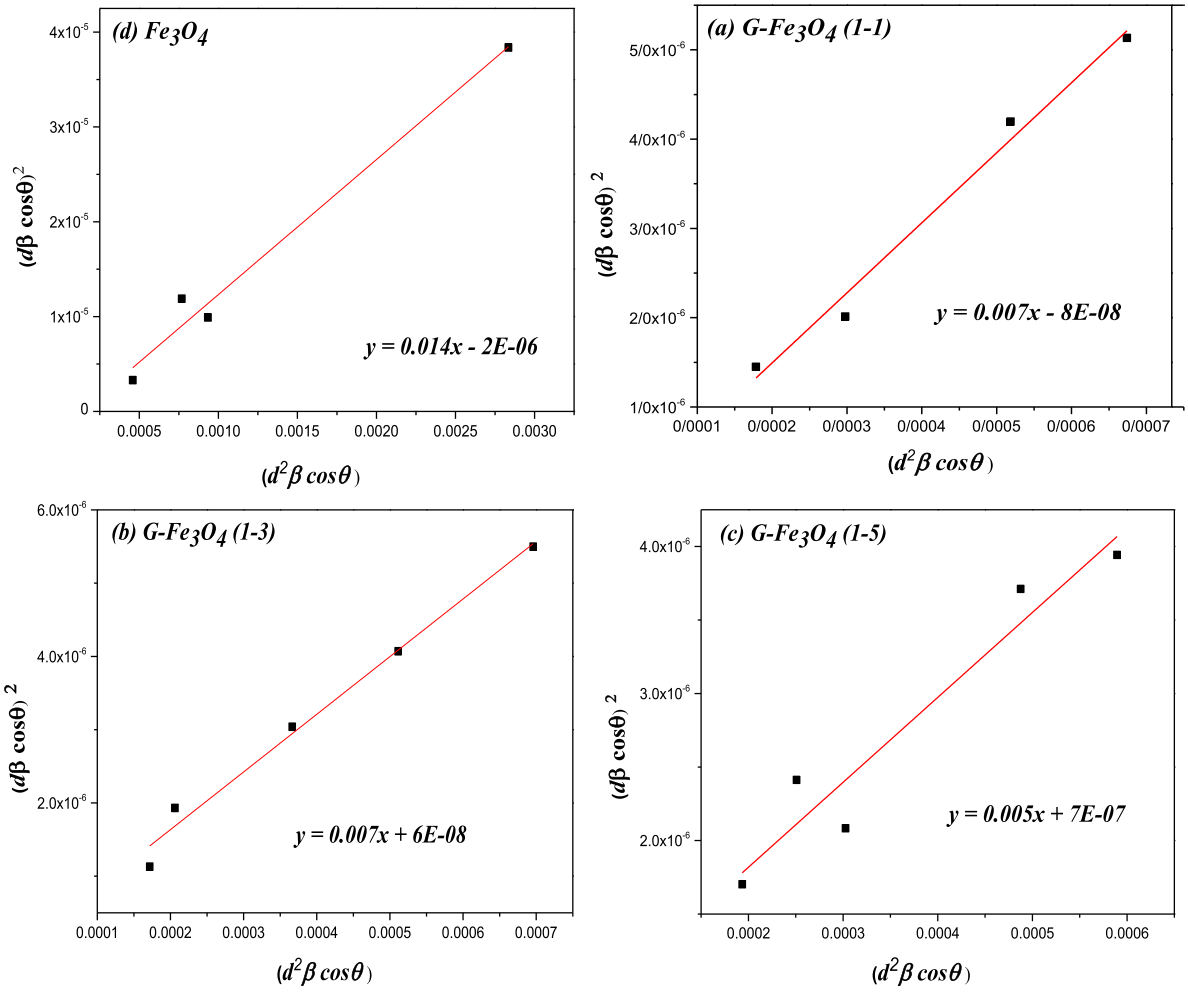

Fig. 2. The SSP plots of the prepared samples.

specific surface area of graphene (2630 m^2g^{-1}) makes it a good supporting material to be decorated with NPs with rather good distribution [14–16]. The graphene based composites exhibit unique mechanical, thermal [17] and electronic properties as well as excellent aqueous processability [18]. In addition, the physico-chemical properties of graphene-based structures including size, stability [19], electrical conductivity [20] and density of functional groups, can be tailored to optimize their applications.

The main purpose of this work was to synthesize a composite having the highest antibacterial activity and the least cytotoxicity. So Fe_3O_4 NPs and graphene-Fe_3O_4 nanocomposites (with different GO/Fe_3O_4 ratios) were both synthesized by the same route (solvothermal), which is a low cost and more convenient method comparing to the others that may need some specific conditions such as using N_2 gas, freeze drying and reflux process [8,21].

Graphene was used as a support for Fe_3O_4 NPs to be distributed on its surface, expecting to increase the effective area which in turn could improve the interaction of the nanocomposite with the bacteria. In addition, since Fe_3O_4 NPs have good magnetic properties, the nanocomposite can easily be removed from the solution using a magnet, after finishing their antibacterial performance. Also, PVP was used to protect the surface and improve the stability of the Fe_3O_4 NPs as well as reducing the cytotoxicity of the nanoparticles [22,23]. The effect of different GO/Fe_3O_4 ratios on the structural, optical and antibacterial properties of the prepared nanocomposites were studied and compared. The antibacterial activity of the prepared samples were investigated using three different methods: (i) broth microdilution method (in liquid medium) measuring minimum inhibitory concentration (MIC), (ii) bacteria growth inhibition rate (the bacterial density is measured with respect to time), (iii) colony counting method, which is done in agar medium.

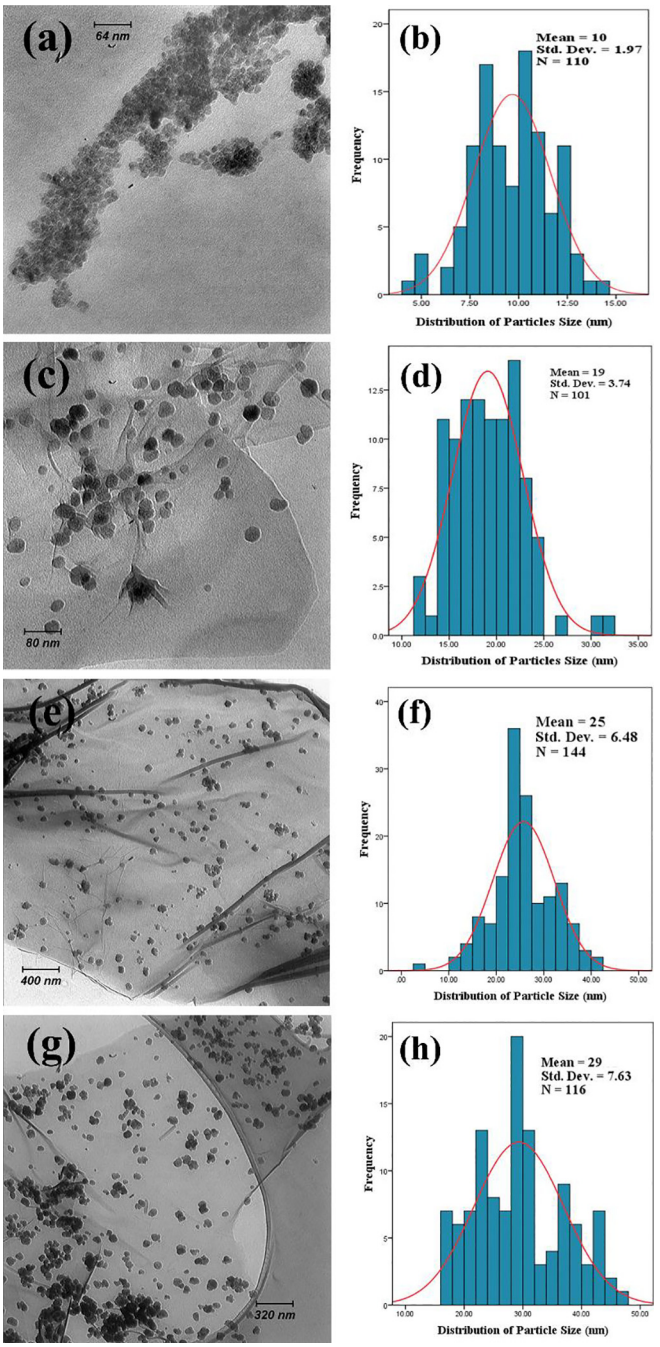

Fig. 3. TEM images and the corresponding histograms of (a,b) Fe_3O_4 nanoparticles, (c,d) 1-1, (e,f) 1–3 and (g,h) 1–5 G-Fe_3O_4 nanocomposites.

2. Experimental

2.1. Materials and method

The starting materials used for the synthesis of G-Fe_3O_4 nanocomposites and Fe_3O_4 nanoparticles were ammonium acetate (NH_4Ac, 99.9% purity, Sigma Aldrich), iron (III) acetylacetonate ($Fe(acac)_3$, Merck), polyvinylpyrrolidone (PVP) and ethyleneglycol (EG, Extra pure, Assay 99%) as the solvent. Graphene oxide (GO) was prepared using the modified Hummer method based on an earlier published report [24]. In order to synthesize GO/Fe_3O_4 with 1-1 ratio, 45 mg of GO was first dispersed in 45 ml EG. Then, 45 mg of $Fe(acac)_3$, as an iron source, was added to GO/EG solution and sonicated for 30 min. After adding NH_4Ac (1.5 g), the obtained mixture was stirred and sealed in a Teflon –lined stainless steel autoclave, maintained at 180 °C for 24 h. The produced solution was centrifuged and washed with deionized water several times and then dried in an oven at 60 °C for about 20 h to obtain the final product.

A similar approach, with the proper amount of $Fe(acac)_3$, was used to prepare G-Fe_3O_4 nanocomposites with 1–3, 1–5 ratios. To synthesize Fe_3O_4 NPs, 0.55 g of $Fe(acac)_3$ and 1.00 g of PVP were added to 25.00 ml EG. The mixture was stirred vigorously at room temperature and then sealed in a Teflon–lined stainless steel

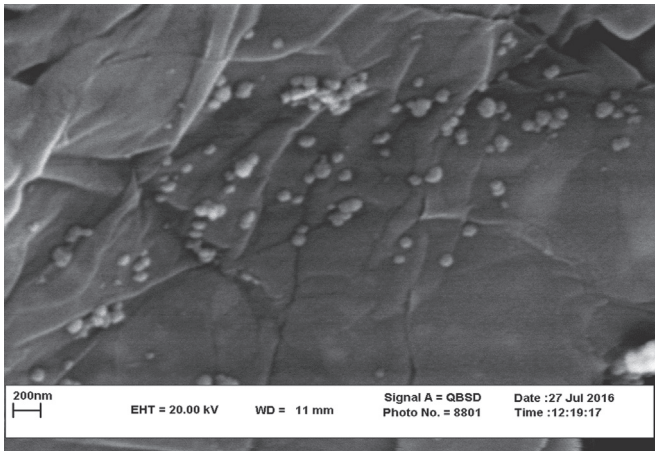

Fig. 4. The SEM image of G-Fe_3O_4 (1–5) nanocomposite.

autoclave and maintained at 180 °C for 12 h. The obtained black solution was washed with acetone, absolute ethanol and deionized water and finally dried at 60 °C for 6 h.

2.2. Characterization

The structure of the synthesized samples was studied by X-ray diffraction (XRD, X'Pert PRO MPD, with Cukα radiation λ = 0.15418 nm). The FTIR spectra were recorded to investigate the chemical interactions between GO and the magnetic Fe_3O_4 NPs. The size of the Fe_3O_4 NPs and the morphology of the prepared samples were examined using transmission electron microscopy (TEM, Leo 912 AB-Germany). Also scanning electron microscopy (SEM, Leo 450 vp) was used to determine any changes of the bacteria's morphology and their destruction mechanisms. Zeta potential and surface charge of the samples were measured by a zeta sizer (CAD zeta compact, France).

3. Results and discussion

3.1. Structure analysis

The XRD patterns of the synthesized G-Fe_3O_4 nanocomposites and Fe_3O_4 NPs are presented in Fig. 1. The small hump, which is seen in the patterns of G-Fe_3O_4 nanocomposites at around 25°, is assigned to graphene sheets. The XRD patterns confirmed the reduction of GO and the presence of Fe_3O_4 NPs in the nanocomposites. These spectra also indicated that the structure of G-Fe_3O_4 nanocomposites and Fe_3O_4 NPs had been formed, corresponding to the databases JCPDS (PDF code: 89-0691for G-Fe_3O_4 and PDF code: 75–1609 for Fe_3O_4) [21,25]. Also, the XRD patterns showed that by decreasing GO/Fe_3O_4 ratio, the peak intensity related to Fe_3O_4 increases. The average crystallite size of the prepared samples were estimated using the Scherrer formula ($D = k\lambda/\beta \cos\theta$), and also calculated by the size-strain plot (SSP) method [26], accordingly:

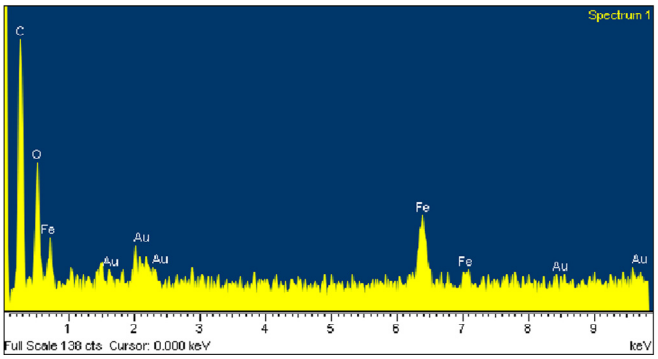

Fig. 6. The EDX analysis of G-Fe_3O_4 (1–5) nanocomposite.

$$(d\beta \cos\theta)^2 = \frac{K}{D}\left(d^2\beta \cos\theta\right) + \left(\frac{\varepsilon}{2}\right)^2 \quad (1)$$

where K is a constant which depends on the shape of the particles, β is the FWHM of the diffraction peaks, d the plane's spacing, θ the diffraction peak angle and λ the X-ray wavelength. In order to obtain the average crystallite size and the lattice strain, using the SSP method the term $(d\beta\cos\theta)^2$ is plotted against $d^2\beta\cos\theta$. The crystallite size is then calculated from the slope of the linearly fitted data, and the lattice strain from the y-intercept, as shown in Fig. 2. The results are given in Table 1. As can be seen, the average crystallite size of Fe_3O_4 increases with an increase of Fe_3O_4 in G-Fe_3O_4 nanocomposites.

The TEM images of the prepared samples and the size

Table 2
The minimum inhibitory concentration (MIC) of the samples against the bacteria.

Compound	*E.coli*	*S.aureus*
MIC of G-Fe_3O_4 (ppm)	100	200
MIC of GO (ppm)	125	225
MIC of Fe_3O_4 (ppm)	150	300

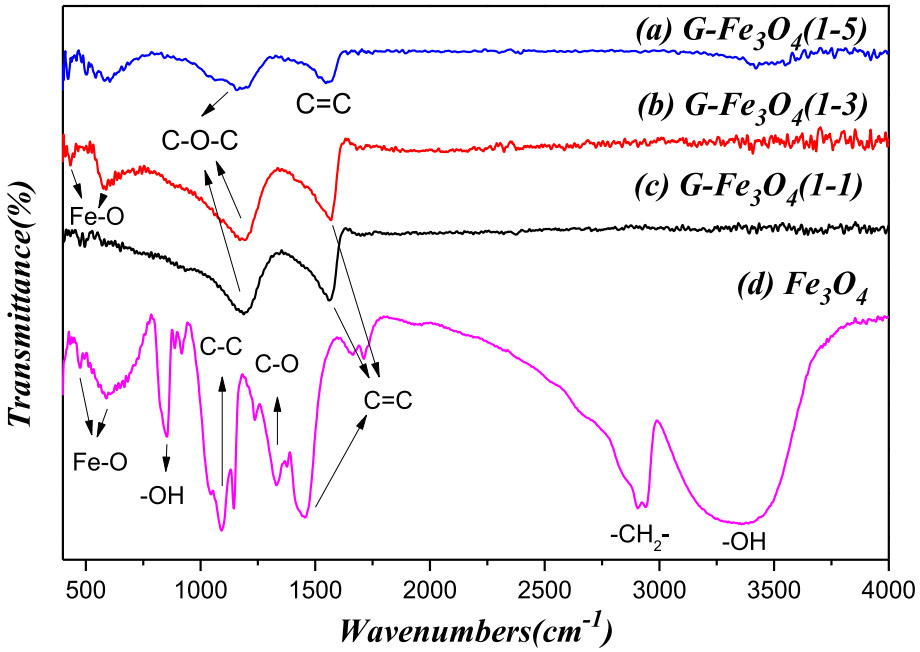

Fig. 5. FTIR spectra of the synthesized G-Fe_3O_4 nanocomposites and Fe_3O_4 nanoparticles.

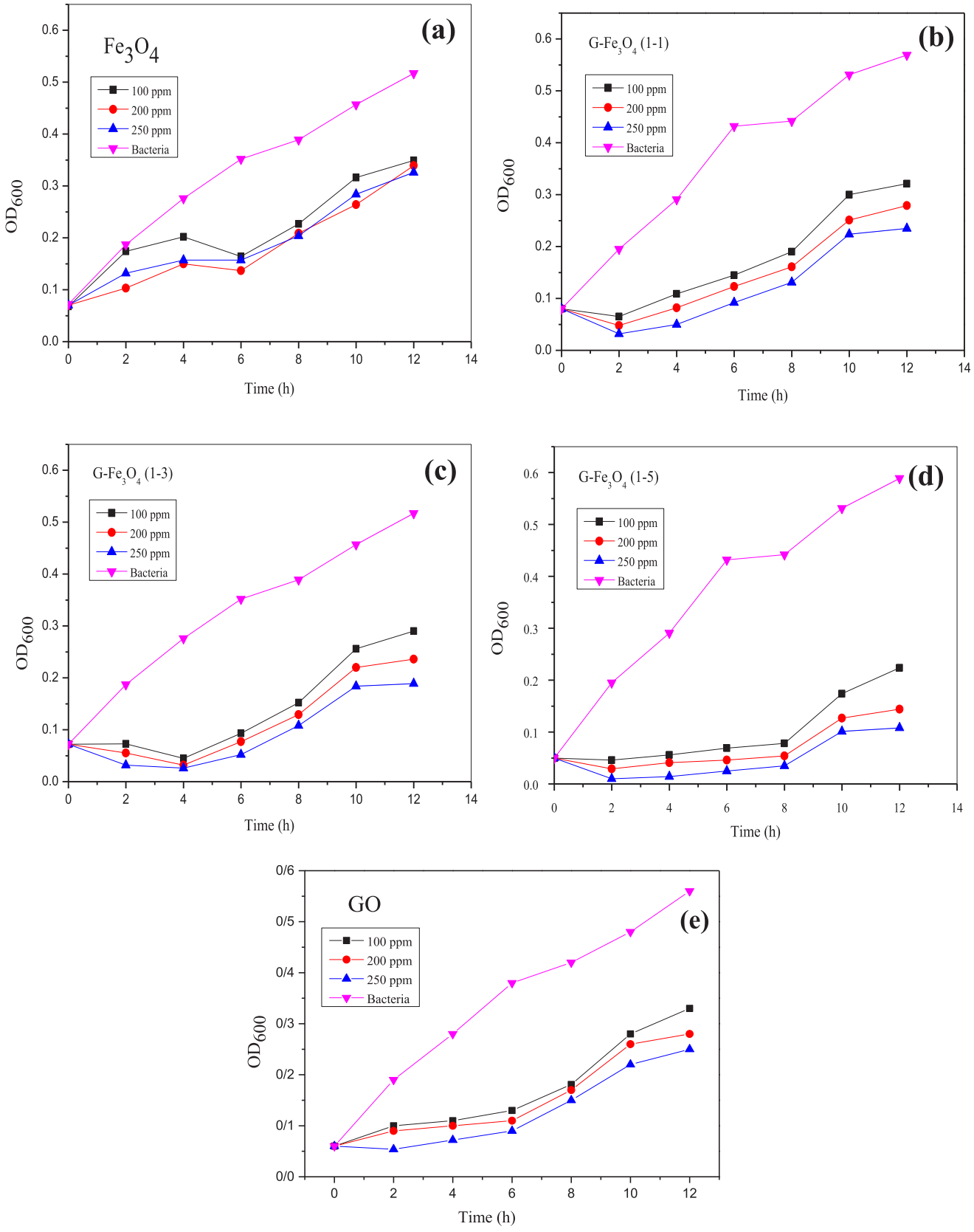

Fig. 7. The growth curves of *E. coli* cells (10^8 CFU/ml) exposed to (a) Fe_3O_4 NPs, (b) G- Fe_3O_4 (1-1), (c) G- Fe_3O_4 (1–3), (d) G- Fe_3O_4 (1–5) nanocomposites and (e) GO.

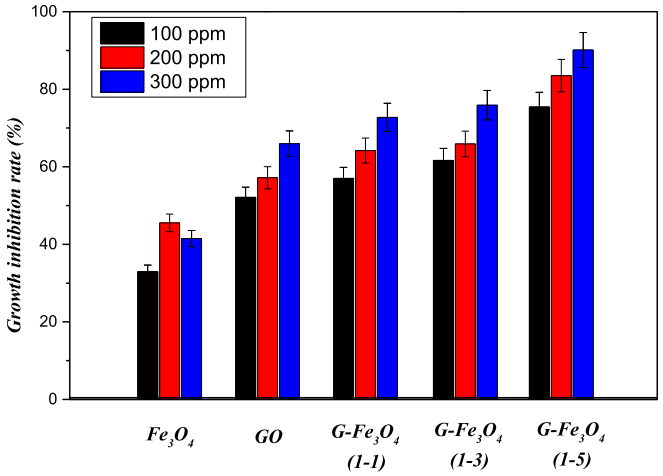

Fig. 8. The growth inhibition rate of *E. coli* bacteria exposed to prepared samples at 37 °C, with different concentrations.

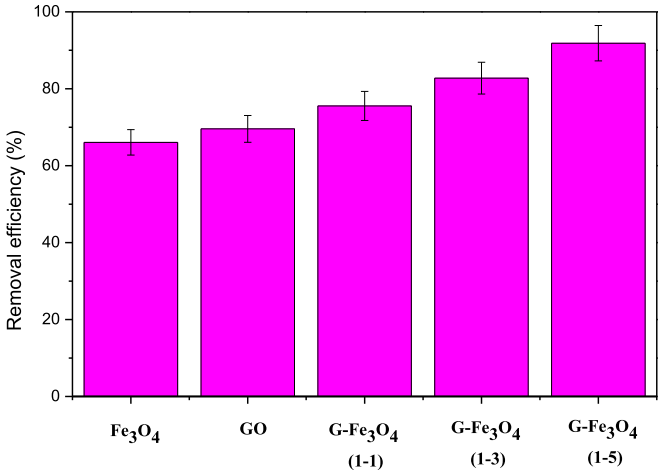

Fig. 10. The removal efficiency of the samples at 250 ppm concentration.

distribution histograms are presented in Fig. 3. Fig. 3b, c and d show that the surface of the graphene sheets are decorated by Fe_3O_4 nanoparticles having a spherical shape. The average particle size of Fe_3O_4 NPs on the graphene sheets in G-Fe_3O_4 (1-1), (1–3) and (1–5) ratios are about 19, 25 and 29 nm, respectively. From Fig. 3a the average particle size of Fe_3O_4 NPs was obtained about 10 nm. The SEM image of the G-Fe_3O_4 (1–5) nanocomposite is given in Fig. 4, which shows that the graphene sheets are well decorated with Fe_3O_4 nanoparticles.

The FTIR spectra of G-Fe_3O_4 nanocomposites and Fe_3O_4 NPs are presented in Fig. 5. The bands at 589 and 460 cm^{-1} are attributed to Fe–O vibrations, which confirm the presence of Fe_3O_4 [27]. In this Fig, the bands at 1197.1 and 1557.1 cm^{-1} are assigned to C–O–C and C=C groups, respectively. In the spectrum of Fe_3O_4 NPs, the bands at 853.5 cm^{-1} and the wide region absorption band around 3359.4 cm^{-1} are both related to the hydroxyl stretching vibrations of OH groups. In addition, the peaks at about 1089,1328,1449 and 2929.3 cm^{-1} belong to the stretching vibrations of C–C, C–O, C=C and $-CH_2$, respectively, which can be related to the presence of PVP surfactant in the Fe_3O_4 NPs, remained from the synthesis process [28].

The EDX spectrum of G-Fe_3O_4 (1–5) nanocomposite, presented in Fig. 6, confirms the existence of Fe, O and C in the prepared samples. The Au in the spectrum is related to the sample coating for the analysis and does not exist in the structure.

3.2. Antibacterial tests

The antibacterial activity of G-Fe_3O_4 nanocomposites with different GO/Fe_3O_4 weight ratios as well as Fe_3O_4 NPs and GO were investigated against Gram negative *E. coli* and Gram positive *S. aureus* as model bacteria. Microtiter plate and growth curve methods were used for measuring the minimum inhibitory concentration (MIC) and the growth inhibition rate, respectively. To measure the viable cells (CFU), the colony counting method was applied. For preparing the bacterial samples, the bacteria were grown in nutrient broth at 37 °C overnight to yield a cell count of approximately 10^8 CFU/ml.

3.2.1. Measurement of minimum inhibitory concentration (MIC)

The MIC of synthesized samples for *E. coli* and *S. aureus* bacteria was determined using microtiter plate technique. Different concentrations of the synthesized samples (50, 100, 150, 200, 300, 400 ppm) were prepared in deionized water. First, 70 μl of the nanocomposites, GO or Fe_3O_4 NPs in dispersed form was inoculated with 70 μl of the tested bacteria at a concentration of 10^8 CFU/ml. The MIC was read after 17, 20, 24 and 48 h of incubation at 37 °C (Table 2). Our results showed that G-Fe_3O_4 (1–5) nanocomposite had a stronger antibacterial effect on *E. coli* and *S. aureus* compared to GO and Fe_3O_4 NPs. This can be due to the larger surface area of the graphene and good distribution of Fe_3O_4 NPs, leading to better interaction between Fe_3O_4 NPs and the bacteria. In addition, since the synthesized samples had stronger antibacterial effects on *E. coli* compared to *S. aureus*, the other antibacterial tests were performed only on *E. coli*. Tan et al. have prepared poly-*l*-lysine/reduced graphene oxide/copper nanoparticles (PLL–rGO–CuNPs) hybrid by anchoring the CuNPs on the reduced graphene oxide surface. The MIC of the prepared samples were also determined by two-fold diluting method. As they reported, the MIC of rGO and PLL–rGO–CuNPs were about 10000 and 300 mg/L, respectively [29].

3.2.2. Bacteria growth inhibition rate

Another antibacterial test was carried out by plotting the growth curve of *E. coli* in a nutrient broth medium in the presence of G-Fe_3O_4 nanocomposites and also Fe_3O_4 NPs and GO with different concentrations (100, 200, 250 ppm). In this test, 100 μl of the *E. coli*

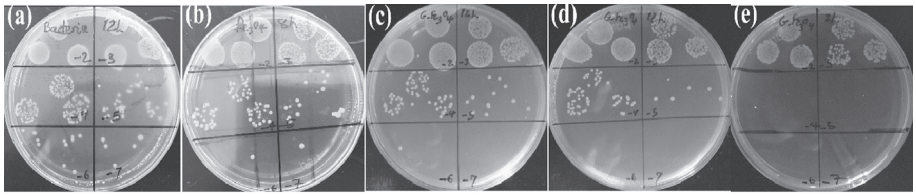

Fig. 9. Some nutrient agar plates that show the inhibition of colonies (a) before treatment and after treatment with (b) Fe_3O_4 NPs, (c) G- Fe_3O_4 (1-1), (d) G- Fe_3O_4 (1–3), (e) G- Fe_3O_4 (1–5).

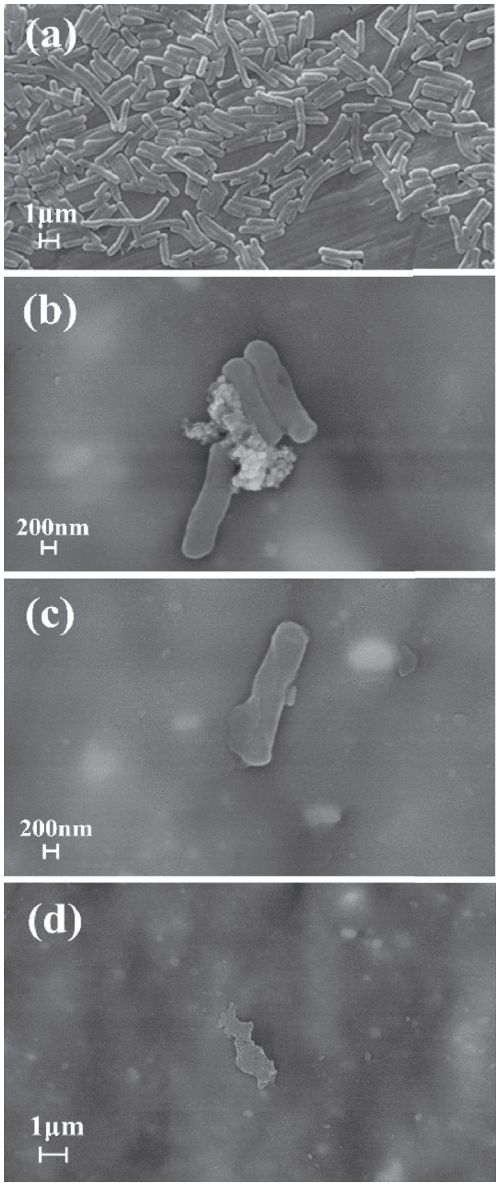

Fig. 11. The SEM images of *E. coli* (a) before the antibacterial tests, (b, c, d) after treatment with a G- Fe_3O_4 nanocomposite.

culture (10^8 CFU/ml) was added to 10 ml of the nutrient broth medium containing a certain concentration of the sterile prepared samples. The mixed solutions were incubated at 30 °C in a rotary shaker at 200 rpm for 12 h. Optical density (OD) of all solutions were measured at 600 nm in 2 h periodicals using spectrophotometry. A blank nutrient broth medium and bacteria solution, in the absence of the synthesized samples and cultured under the same conditions, were used as the positive and negative controls. The growth curves of *E. coli* in the presence and absence of 3 different concentrations of G-Fe_3O_4 nanocomposites, Fe_3O_4 NPs and GO, are shown in Fig. 7. The bacterial growth inhibition rates were calculated, according to the following relation

$$\textit{Bacterial growth inhibition rate} = \left(1 - \frac{\text{OD}_{600} \text{ of bacteria in presence of sample}}{\text{OD}_{600} \text{ of positive control}}\right) \times 100 \quad (2)$$

Our results showed that all the samples had antibacterial effects on *E. coli* (Fig. 8). However, Fe_3O_4 NPs with 200 ppm concentration inhibited the bacterial growth by 45.5%, which is higher than that of 250 ppm (41.4%). Since Fe_3O_4 NPs have magnetic properties, they usually agglomerate and their effective surface area decreases. This leads to the reduction of the interaction between the Fe_3O_4 NPs and the bacteria cell wall, which in turn results in lower bacterial growth inhibition. The bacterial growth inhibition of G-Fe_3O_4 nanocomposite (1–5) at concentrations of 100 and 200 ppm were 75.66% and 83.5%, respectively. Also, it was found that the cell viability of *E. coli* progressively decreased with an increase in G-Fe_3O_4 concentration. Sun et al. have studied the time course of antibacterial activity by GO, CdS and GO-CdS towards *E. coli*. Their results showed that GO had limited activity in inactivating *E. coli*. Furthermore, GO-CdS composites show more enhanced antibacterial activity than CdS nanoparticles [30].

3.2.3. Colony counting method

To examine the bactericidal effects of Fe_3O_4 NPs, GO and G-Fe_3O_4 nanocomposites on *E. coli* more accurately, the bacteria with a concentration of 10^8 (CFU/ml) were cultured on nutrient agar plates supplemented with the synthesized samples at concentration of 250 ppm. Nutrient agar plates without the samples, cultured under the same conditions, were used as a control and each colonization test was run in triplicate and repeated at 6 separate times. The plates were incubated for 24 h at 37 °C and the number of colonies was enumerated. The counts on three plates, corresponding to a particular sample, were averaged. Fig. 9 shows some nutrient agar plates that describe the inhibition of colony growth after the sample treatment during 12 h incubation. The removal efficiency of the bacteria by Fe_3O_4 NPs, GO and G-Fe_3O_4 nanocomposites were calculated according to the following formula:

$$\textit{removal efficiency}\ (\%) = \frac{CFU_0 - CFU_t}{CFU_0} * 100 \quad (3)$$

where CFU_0 and CFU_t are the initial and residual numbers of the bacterial colonies in the presence of the prepared samples. Park and co-workers synthesized ZnO-graphene nanoparticle hybrids by coating ZnO on the graphene sheets and studied their antibacterial activity by colony forming count method. A complete decline of the bacteria was achieved after 12 h, at concentration of o. oo3 g/ml [31]. Also, Kollu et al. synthesized G-Fe_3O_4 nanocomposite by solvothermal method and measured the antibacterial activity with the same method. The TEM images of the prepared nanocomposites revealed that the size of the Fe_3O_4 particles on the surface of the graphene was in the range of 0.2–0.25 μm. They reported that the removal efficiency of the cells by G-Fe_3O_4 and GO were 77% and 35%, respectively [32]. Our results for the samples with 250 ppm concentration (Fig. 10) indicated that among all the samples, G-Fe_3O_4 (1–5) nanocomposite with 92.1% and Fe_3O_4 NPs with 66.4% had the highest and the least inhibition growth effects on *E. coli*, respectively.

3.2.4. Mechanisms of the antibacterial action

To better understand the influence of G-Fe_3O_4 nanocomposite on *E. coli* cells, SEM analysis was performed on the bacteria sample in the presence and absence of the G-Fe_3O_4 nanocomposites. SEM

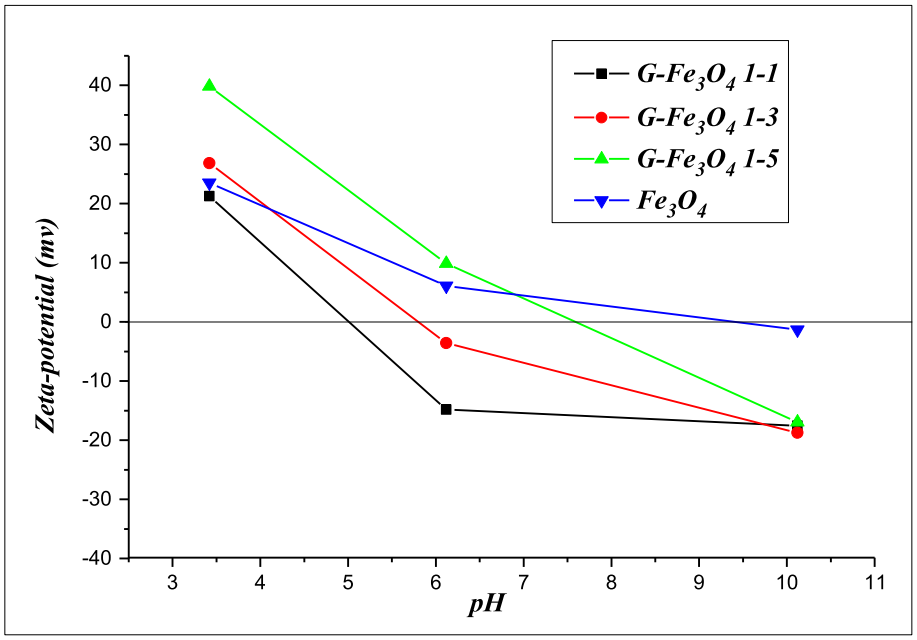

Fig. 12. Zeta potential of the prepared samples vs. pH.

electron micrograph images before and after the treatment by a G-Fe_3O_4 nanocomposite (Fig. 11) showed that the nanoparticles had been accumulated in the cell envelopes. This resulted in the formation of pits (Fig. 11c) and further devastating damages of the bacteria (Fig. 11d). The G-Fe_3O_4 nanocomposite-bacteria interactions could be interpreted through 3 mechanisms. The first approach can be via the electrostatic interaction between positively charged G-Fe_3O_4 nanocomposite and negatively charged residues of the membrane proteins on the bacterial surface. The second approach can be the physicochemical changes in the bacterial cell wall and the last mechanism might be due to the penetration of Fe_3O_4 NPs through bacterial membranes which can disorganize the intracellular activities of the bacteria cells [33]. Nanocomposites based on graphene affect the bacterial membrane through direct contact and oxidative stress. Also, it has been reported that the oxidative stress of rGO is more than that of GO. The density of functional groups in graphene based materials is rather high, so having more chances to interact with the bacteria [34].

3.2.5. Zeta potential analysis

Zeta potential measurement is a significant strength predictor regarding the electrostatic interaction between the nanoparticles and the bacteria cells. Since zeta potential can be affected by pH, the zeta potential of the samples was measured at different pH levels

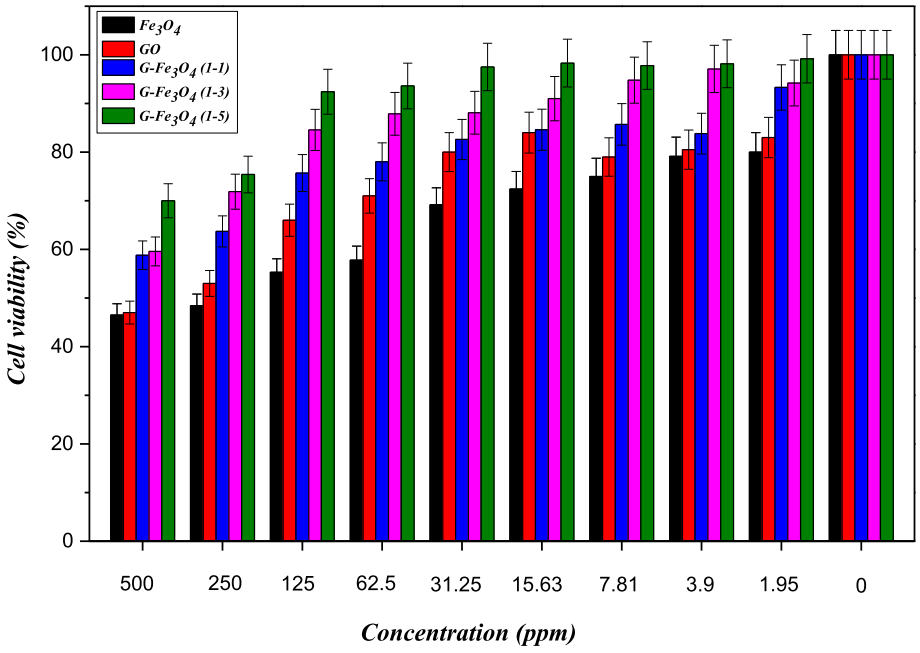

Fig. 13. Relative cell viability of synthesized samples against N2A cells at different concentrations.

(4.5, 6.5 and 10), which are given in Fig. 12. As mentioned earlier, the bacterial removal efficiency of the G-Fe_3O_4 (1–5) nanocomposite is higher than that of the Fe_3O_4 NPs. This can be due to the stronger surface charge of the G-Fe_3O_4 (1–5) nanocomposites at a neutral pH, resulting in a stronger electrostatic interaction with the gram negative *E. coli* bacteria.

3.2.6. Biocompatibility assessment: MTT assay method

To evaluate the biocompatibility of our synthesized samples, the cytotoxic activity of the samples was investigated by MTT assay in Neuroblastoma cells (N2A). According to the standard MTT assay, the cells were incubated at 37 °C for 24 h under various concentrations (1.95–500 ppm) of the samples. As shown in Fig. 13, the cell viability is found to be more than 70% for G-Fe_3O_4 (1–5) nanocomposite at concentrations of 500 ppm and lower, indicating that G-Fe_3O_4 (1–5) nanocomposite has low toxicity. The Fe_3O_4 NPs with the least cell viability are more toxic, compared to the other prepared samples. These results can be related to the size of NPs. Since the effective surface area of the particles is an important parameter in determining the toxicity of NPs, so it seems that the smaller NPs are more toxic [35,36]. It has been reported that decorating the surface of rGO with nanoparticles modifies the surface and decreases the toxicity comparing to GO [37]. The presence of oxygen containing functional groups at the edges of the graphene sheet folds the sharp edges, which results in reducing the damages to the cell [38].

4. Conclusion

G-Fe_3O_4 nanocomposites, with different weight ratios of GO/Fe_3O_4 (1-1, 1–3 and 1–5) as well as Fe_3O_4 NPs were synthesized using the solvothermal method. The XRD patterns confirmed the formation of the desired structures. The average size of the crystallites was determined using the Scherrer formula and SSP method. TEM images showed that the average particle size of Fe_3O_4 NPs in the G-Fe_3O_4 nanocomposites of 1-1, 1–3 and 1–5 are about 19, 25 and 29 nm, respectively. Also, the average size of the synthesized Fe_3O_4 NPs was found to be 10 nm. SEM images indicated that the Fe_3O_4 NPs are anchored on the surface of the graphene sheets. To investigate the antibacterial property of the prepared samples, the Minimum Inhibitory Concentration method (MIC) was employed. By using the colony counting method, the average growth inhibition rate of *E. coli* bacteria for the Fe_3O_4 NPs, GO and G-Fe_3O_4 1-1, 1–3 and 1–5 nanocomposites at a concentration of 250 ppm were obtained 66.4%, 69.7%, 75.6%, 82.8%, 92.1%, respectively. These results showed that the G-Fe_3O_4 (1–5) nanocomposite has the higher antibacterial activity and lower cytotoxicity, in comparison with the other synthesized samples.

Acknowledgement

The authors would like to thank Dr. M. Darroudi from Mashhad University of Medical Sciences for doing the toxicity tests.

References

[1] X. Xin, Q. Wei, J. Yang, L. Yan, R. Feng, G. Chen, B. Du, H. Li, Highly efficient removal of heavy metal ions by amine-functionalized mesoporous Fe 3 O 4 nanoparticles, Chem. Eng. J. 184 (2012) 132–140.
[2] T. Zhu, J.S. Chen, X.W. Lou, Highly efficient removal of organic dyes from waste water using hierarchical NiO spheres with high surface area, J. Phys. Chem. C 116 (2012) 6873–6878.
[3] K. Kabra, R. Chaudhary, R.L. Sawhney, Treatment of hazardous organic and inorganic compounds through aqueous-phase photocatalysis: a review, Ind. Eng. Chem. Res. 43 (2004) 7683–7696.
[4] J. Kim, B. Van der Bruggen, The use of nanoparticles in polymeric and ceramic membrane structures: review of manufacturing procedures and performance improvement for water treatment, Environ. Pollut. 158 (2010) 2335–2349.
[5] T.A. Dankovich, D.G. Gray, Bactericidal paper impregnated with silver nanoparticles for point-of-use water treatment, Environ. Sci. Technol. 45 (2011) 1992–1998.
[6] J. Helmlinger, C. Sengstock, C. Groß-Heitfeld, C. Mayer, T. Schildhauer, M. Köller, M. Epple, Silver nanoparticles with different size and shape: equal cytotoxicity, but different antibacterial effects, RSC Adv. 6 (2016) 18490–18501.
[7] D.K. Tiwari, J. Behari, P. Sen, Application of Nanoparticles in Waste Water Treatment 1, 2008.
[8] Z.-S. Wu, S. Yang, Y. Sun, K. Parvez, X. Feng, K. Müllen, 3D nitrogen-doped graphene aerogel-supported Fe3O4 nanoparticles as efficient electrocatalysts for the oxygen reduction reaction, J. Am. Chem. Soc. 134 (2012) 9082–9085.
[9] X.-M. Li, G. Xu, Y. Liu, T. He, Magnetic Fe3O4 nanoparticles: synthesis and application in water treatment, Nanosci. Nanotechnol. - Asia 1 (2011) 14–24.
[10] X. Wang, R. Zhang, C. Wu, Y. Dai, M. Song, S. Gutmann, F. Gao, G. Lv, J. Li, X. Li, The application of Fe3O4 nanoparticles in cancer research: a new strategy to inhibit drug resistance, J. Biomed. Mater. Res. Part A 80 (2007) 852–860.
[11] S. Xuan, F. Wang, J.M. Lai, K.W. Sham, Y.-X.J. Wang, S.-F. Lee, J.C. Yu, C.H. Cheng, K.C.-F. Leung, Synthesis of biocompatible, mesoporous Fe3O4 nano/microspheres with large surface area for magnetic resonance imaging and therapeutic applications, ACS Appl. Mater. Interfaces 3 (2011) 237–244.
[12] Y. Zhang, X. Liang, X. Yang, H. Liu, J. Yao, An eco-friendly slow-release urea fertilizer based on waste mulberry branches for potential agriculture and horticulture applications, ACS Sustain. Chem. Eng. 2 (2014) 1871–1878.
[13] P.K. Boruah, D.J. Borah, J. Handique, P. Sharma, P. Sengupta, M.R. Das, Facile synthesis and characterization of Fe 3 O 4 nanopowder and Fe 3 O 4/reduced graphene oxide nanocomposite for methyl blue adsorption: a comparative study, J. Environ. Chem. Eng. 3 (2015) 1974–1985.
[14] J.Z. Wang, C. Zhong, D. Wexler, N.H. Idris, Z.X. Wang, L.Q. Chen, H.K. Liu, Graphene-encapsulated Fe3O4 nanoparticles with 3D laminated structure as superior anode in lithium ion batteries, Chem.-A Eur. J. 17 (2011) 661–667.
[15] L. Feng, Z. Liu, Graphene in biomedicine: opportunities and challenges, Nanomedicine 6 (2011) 317–324.
[16] H. Zhang, G. Grüner, Y. Zhao, Recent advancements of graphene in biomedicine, J. Mater. Chem. B 1 (2013) 2542–2567.
[17] J.D. Renteria, D.L. Nika, A.A. Balandin, Graphene thermal properties: applications in thermal management and energy storage, Appl. Sci. 4 (2014) 525–547.
[18] D. Li, M.B. Müller, S. Gilje, R.B. Kaner, G.G. Wallace, Processable aqueous dispersions of graphene nanosheets, Nat. Nanotechnol. 3 (2008) 101–105.
[19] V. Brus, M. Gluba, X. Zhang, K. Hinrichs, J. Rappich, N. Nickel, Stability of graphene–silicon heterostructure solar cells, Phys. Status Solidi 211 (2014) 843–847.
[20] H. Kim, Y. Miura, C.W. Macosko, Graphene/polyurethane nanocomposites for improved gas barrier and electrical conductivity, Chem. Mater. 22 (2010) 3441–3450.
[21] W. Lü, Y. Wu, J. Chen, Y. Yang, Facile preparation of graphene–Fe 3 O 4 nanocomposites for extraction of dye from aqueous solution, CrystEngComm 16 (2014) 609–615.
[22] W. Wang, Q. Chen, C. Jiang, D. Yang, X. Liu, S. Xu, One-step synthesis of biocompatible gold nanoparticles using gallic acid in the presence of poly-(N-vinyl-2-pyrrolidone), Colloid. Surface. Physicochem. Eng. Aspect. 301 (2007) 73–79.
[23] N. Haberl, S. Hirn, A. Wenk, J. Diendorf, M. Epple, B.D. Johnston, F. Krombach, W.G. Kreyling, C. Schleh, Cytotoxic and proinflammatory effects of PVP-coated silver nanoparticles after intratracheal instillation in rats, Beilstein J. Nanotechnol. 4 (2013) 933.
[24] S.A. Khayatian, A. Kompany, N. Shahtahmassebi, A.K. Zak, Preparation and characterization of Al doped ZnO NPs/graphene nanocomposites synthesized by a facile one-step solvothermal method, Ceram. Int. 42 (2016) 110–115.
[25] H. El Ghandoor, H. Zidan, M.M. Khalil, M. Ismail, Synthesis and some physical properties of magnetite (Fe3O4) nanoparticles, Int. J. Electrochem. Sci. 7 (2012) 5734–5745.
[26] A.K. Zak, W.A. Majid, M.E. Abrishami, R. Yousefi, X-ray analysis of ZnO nanoparticles by Williamson–Hall and size–strain plot methods, Solid State Sci. 13 (2011) 251–256.
[27] J. Su, M. Cao, L. Ren, C. Hu, Fe3O4–graphene nanocomposites with improved lithium storage and magnetism properties, J. Phys. Chem. C 115 (2011) 14469–14477.
[28] L. Xiaojuana, J. Guoyuanb, Z. Lipingb, Y. Yuxiangb, L. Xiangnongc, Synthesis and properties of Fe3O4 nanoparticles by Sol vothermal method using iron (iii) Acetylacetonate1, Glass Phys. Chem. 37 (2011) 459–465.
[29] Y. Ouyang, X. Cai, Q. Shi, L. Liu, D. Wan, S. Tan, Y. Ouyang, Poly-l-lysine-modified reduced graphene oxide stabilizes the copper nanoparticles with higher water-solubility and long-term additively antibacterial activity, Colloids Surfaces B Biointerfaces 107 (2013) 107–114.
[30] P. Gao, J. Liu, D.D. Sun, W. Ng, Graphene oxide–CdS composite with high photocatalytic degradation and disinfection activities under visible light irradiation, J. Hazard Mater. 250 (2013) 412–420.
[31] T. Kavitha, A.I. Gopalan, K.-P. Lee, S.-Y. Park, Glucose sensing, photocatalytic and antibacterial properties of graphene–ZnO nanoparticle hybrids, Carbon 50 (2012) 2994–3000.
[32] C. Santhosh, P. Kollu, S. Doshi, M. Sharma, D. Bahadur, M.T. Vanchinathan,

P. Saravanan, B.-S. Kim, A.N. Grace, Adsorption, photodegradation and antibacterial study of graphene–Fe 3 O 4 nanocomposite for multipurpose water purification application, RSC Adv. 4 (2014) 28300–28308.
[33] S. Agnihotri, S. Mukherji, S. Mukherji, Size-controlled silver nanoparticles synthesized over the range 5–100 nm using the same protocol and their antibacterial efficacy, RSC Adv. 4 (2014) 3974–3983.
[34] A.M. Pinto, I.C. Goncalves, F.D. Magalhães, Graphene-based materials biocompatibility: a review, Colloids Surfaces B Biointerfaces 111 (2013) 188–202.
[35] M.V. Park, A.M. Neigh, J.P. Vermeulen, L.J. de la Fonteyne, H.W. Verharen, J.J. Briedé, H. van Loveren, W.H. de Jong, The effect of particle size on the cytotoxicity, inflammation, developmental toxicity and genotoxicity of silver nanoparticles, Biomaterials 32 (2011) 9810–9817.
[36] D. Napierska, L.C. Thomassen, V. Rabolli, D. Lison, L. Gonzalez, M. Kirsch-Volders, J.A. Martens, P.H. Hoet, Size-dependent cytotoxicity of monodisperse silica nanoparticles in human endothelial cells, Small 5 (2009) 846–853.
[37] V.C. Sanchez, A. Jachak, R.H. Hurt, A.B. Kane, Biological interactions of graphene-family nanomaterials: an interdisciplinary review, Chem. Res. Toxicol. 25 (2011) 15–34.
[38] A.M. Pinto, C. Gonçalves, D.M. Sousa, A.R. Ferreira, J.A. Moreira, I.C. Gonçalves, F.D. Magalhaes, Smaller particle size and higher oxidation improves biocompatibility of graphene-based materials, Carbon 99 (2016) 318–329.